DOI:
10.1021/acs.jpcc.7b00973

Document Version
Peer reviewed version

Spectroscopic Fingerprints of Carbon Monomers and Dimers on Ir(111): Experiment and Theory

Francesco Presel[1], Cristian A. Tache[1], Holly Tetlow[2], Davide Curcio[1], Paolo Lacovig[3], Lev Kantorovich[2], Silvano Lizzit[3], Alessandro Baraldi[1,3,4,]*

[1] Physics Department, University of Trieste, Via Valerio 2, 34127 Trieste, Italy

[2] Physics Department, King's College London, London, WC2R 2LS, UK.

[3] Elettra-Sincrotrone Trieste S.C.p.A., Strada Statale 14 Km 163.5, 34149 Trieste, Italy

[4] IOM-CNR, Laboratorio TASC, AREA Science Park, S.S. 14 Km 163.5, 34149 Trieste, Italy.

ABSTRACT

By combining high-resolution photoelectron spectroscopy and ab initio calculations, we show that different carbon clusters can be formed on Ir(111) upon low temperature molecular beam epitaxy using a solid state carbon source. Besides carbon monomers, also dimers, trimers and larger clusters are detected through C 1s core levels measurements. The spectroscopic signal of carbon monomers is then used as a fingerprint to detect their presence during the early stages of graphene growth by ethylene chemical vapor deposition at high temperature. We demonstrate that our spectroscopic approach can be employed to investigate the role of carbon monomers and dimers in the nucleation and growth of graphene on different metal surfaces.

1. Introduction

The interest of the material's science community in carbon monomers (C_1) and dimers (C_2) has grown considerably in the last years because of their role in the synthesis of high-quality graphene (Gr) monolayers on solid surfaces[1-3]. Carbon clusters, especially those formed by a small number of atoms, play an important role in determining the different atomistic mechanisms for the epitaxial growth of graphene by means of chemical vapor deposition (CVD). The carbon monomers' concentration and the rate at which adatoms are generated from the hydrocarbon feedstock are relevant quantities for understanding the non-linear growth kinetics of Gr experimentally observed on different surfaces[4]. The control of monomer supersaturation is an effective approach to modify not only the growth rate, but also the morphology and orientation of the Gr islands[5]. In addition, C monomers are predicted to be essential for the growth of the graphene islands both through direct attachment to the Gr edges and through the formation and attachment of larger C clusters[6].

Apart from monomers, also dimers play an important role in the formation of high-quality Gr monolayers characterized by a low density of defects such as mono- and di-vacancies, disclinations, dislocations, and domain boundaries[7]. For example, according to theoretical calculations, in the case of copper surfaces, where dimers represent the dominant feeding species for Gr growth[8,9], they have either a diffusion- or an attachment-limited aggregation behavior depending on the crystallographic surface orientation[10,11]. More specifically, while the rate determining step for Gr growth on Cu(111) is the energy barrier for dimer surface diffusion, in the case of Cu(100) the limit is given by the energy barrier for the attachment of C_2 to both zig-zag and arm-chair terminated Gr edges. On the other hand, it has been predicted that the formation of dimers is energetically unfavorable on ideal and flat transition metal surfaces (such as Ir and Ru), characterized by a large C-metal bond strength[6]. However, the important role played by dimers in Gr growth has been experimentally established in the case

of stepped Ru(0001)[12,13], Co(0001)[14,15], Ni(111)[16,17] and even for CuNi surface alloys[18]. Besides their relevance for graphene epitaxial growth, C_2 species are extremely important for the formation of all carbon-based three-dimensional materials[19], for the synthesis of carbon quantum dots, and as building blocks for metal-alkynide and alkynide complexes[20,21].

The energetics of monomer and dimer attachment to step edges, which represent the preferred Gr nucleation sites, has been investigated by means of density functional theory (DFT) on different metal surfaces[12]. While the step edges on the Ir(111) surface cannot serve as efficient trapping centers for C_1 adatoms, they can readily facilitate the formation of C_2 dimers. The opposite was found in the case of Cu(111)[12]. Chen *et al.* explained this contrasting behavior as due to the interplay between C-C and C-metal interaction strengths.

The detection of C_1 using spectroscopic approaches is not an easy task and for this reason their presence on solid surfaces has often been revealed by exploiting changes in low energy electron reflectivity[5]. In fact, the diffusion barrier of monomers and dimers is quite low[12], and they can rapidly diffuse and attach to step edges at the temperatures at which high-quality graphene is typically grown on transition metals and their surface density in Gr growing conditions is therefore about a few percent of a monolayer.

In order to overcome these problems and produce a high density of C monomers and dimers in a stable configuration on the Ir(111) surface, we have employed molecular beam epitaxy (MBE) from a graphite target and low temperature deposition (T=80 K). As discussed below this method allowed us to produce several C species that we could reveal and characterize by means of high energy-resolution core level photoelectron spectroscopy supported by DFT calculations. Moreover, the use of a solid-state carbon source is an effective method for growing Gr on substrates where the cracking of precursor molecules used in CVD is hindered[22,23].

The results of this characterization have then been applied for a spectroscopic study of high temperature (T=820 K) ethylene CVD growth of graphene where the C 1s core electron binding energy of C monomers was used as a fingerprint for the detection of the carbon adatom lattice gas which constitutes the C feedstock for Gr growth[5].

2. Experimental Methods

All measurements were performed at the SuperESCA beamline of the Elettra synchrotron radiation facility in Trieste. The experimental chamber is equipped with a 150 mm mean radius SPECS hemispherical electron energy analyzer. The background pressure in the main chamber during measurements was always better than $2x10^{-10}$ mbar. The Ir(111) single crystal was cleaned by Ar^+ sputtering at room temperature (E=1.5 keV), annealing to 1400 K, oxygen cycles to remove residual carbon (in the range 570-1070 K at $p=5x10^{-8}$ mbar) and finally hydrogen treatments to remove residual oxygen traces ($p=5x10^{-8}$ mbar, T=300-770 K). Surface cleanliness was checked by inspecting C 1s, S 2p and O 1s signals and by measuring the Ir $4f_{7/2}$ signal, which is known to show a surface core level shift (CLS) of -550 meV when the surface is clean[24]. Prior to the photoemission measurements, we acquired LEED images of the clean surface, which show intense and narrow integer-order diffraction spots with a low background.

Carbon deposition was carried out at T=80 K by employing electron-beam bombardment on a high-purity graphite rod placed 80 mm from the sample surface, resulting in a carbon flux of 0.07 ML/s. During deposition, the pressure was always kept below $1x10^{-9}$ mbar to prevent surface contamination. The carbon coverage was calibrated by comparing the C 1s photoemission intensity with the one measured for a single layer of graphene on Ir(111) ($3.87 x10^{15}$ atoms/cm^2=2.47 ML), where 1 ML corresponds to one C atom per each Ir substrate atom). The C 1s core level spectra acquired after C deposition by means of MBE were always

measured at hυ=400 eV and at normal emission, with an overall energy resolution of 50 meV, that was previously determined by measuring the broadening of the Fermi edge on a silver crystal. Core level binding energies were always calibrated with respect to the Fermi level. The high-resolution spectra presented in this work were measured at T=80 K in order to reduce the vibrational broadening and enhance the possibility of distinguishing different components, as well as to ensure that the C species were immobile during the whole experiment due to their thermal energy being low with respect to their diffusion and reaction barriers.

The ethylene uptake was performed at high temperature (T=820 K) by using a supersonic molecular beam[25], with a local C_2H_4 pressure of $5x10^{-8}$ mbar. The fast-XPS data acquired during this uptake were measured in real time in snap-shot mode. Since the acquisition time for a single C 1s spectrum is only 500 ms, this method permits to probe *in-situ* the evolution of the different carbon species during the ethylene uptake. Besides the increased number of spectra available over the whole uptake experiment, this operation mode allows a more efficient sampling of the low coverage limit, when we expect to detect the presence of C monomers, according to a previous LEEM investigation[4].

The data analysis was performed by fitting all the C 1s and Ir $4f_{7/2}$ spectra with Doniach-Sunjic (DS) functions[26] convoluted with a Gaussian with full width at half maximum (FWHM) G (which takes into account the broadening due to the vibrational/phonon and inhomogeneous effects and to the instrumental resolution). The DS function is characterized by two parameters: the singularity index α (describing the asymmetry due to e-h pairs excitations) and the Lorentzian width L (due to the finite core-hole lifetime). The inelastic contribution to the photoemission spectra was described with a linear background. The procedure for the determination of the DS lineshape parameters is discussed in detail in Section 4.3.

3. Theoretical methods

The geometry optimization calculations for the carbon clusters were performed using the CP2K code[27]. The Ir(111) surface was represented with an 8 x 8 cell of four layers, and the vacuum gap was greater than 15 Å, to avoid cross-talk effects because of the periodical repetition of the unit cells. Two bottom layers were fixed to the Ir bulk geometry while the upper layers were allowed to relax. For the geometry relaxation calculations the generalized gradient approximation (GGA) was used, along with the PBE exchange-correlation functional[28], Goedecker-Teter-Hutter pseudopotentials[29], and the optimized m-DZVP basis set[30] (with a plane wave cutoff energy of 300 Ry). The DFT-D3 method was used to account for the van der Waals forces[31]. The geometries were relaxed until the force on the atoms was less than 0.038 eV/Å. The size of the Ir(111) cell and the precision thresholds used in our calculations were carefully checked and found sufficient for determining the structural parameters and the adsorption energies with an accuracy better than 0.01 Å and 0.1 eV, respectively.

Formation energies of carbon clusters with *N* atoms were calculated via the formula:

$$\Delta E_{form}(N) = \Delta E(N) - N\Delta E(1),$$

where $\Delta E(N) = E(N) - E_{surf}$ is the difference between the energy of the cluster on the surface, $E(N)$, and the energy of the independently relaxed surface, E_{surf}. Correspondingly, $\Delta E(1)$ is then the binding energy of a single C atom to the surface.

In order to calculate the energy barriers required for removing either a carbon atom or a dimer from an edge of the graphite surface, the Nudged Elastic Band (NEB) was used, with initial structures being a relaxed surface edge, and the final structures containing the removed species placed some distance away from the edge in the vacuum gap between the slabs. The energy in the relaxed bands in all cases was found to increase monotonically between the initial and final states, so that in each case the energy barrier corresponds to the difference between these two states.

The CLS calculations were performed using the Vienna *ab-initio* software package (VASP)[32-34]. The Ir(111) surface consisted of a 4 x 4 cell, again with four layers. The CLS for a particular C atom in a cluster was calculated[35] as the energy difference between the system with a core electron promoted to the valence band, $E(n_c - 1)$, and the energy of the unexcited system $E(n_c)$:

$E_{CLS} = E(n_c - 1) - E(n_c)$.

We have verified that, by using these calculations parameters, we are able to achieve an accuracy in CLSs better than 100 meV.

4. Results and discussion

4.1 Experimental results

Figure 1 shows the sequences of C 1s core level spectra measured after each deposition (thick blue lines) of 0.11 (a), 0.32 (b) and 0.74 ML (c) of carbon and after subsequent annealing to increasing temperatures (thin lines). The spectra measured at T=80 K for both the low (Fig. 1(a)) and medium (Fig. 1(b)) coverage show two major components at about 283.4 eV (M) and 283.9 eV (D). From this first inspection, it appears that at least two non-equivalent species are present on the surface already at low coverage. Besides the M and D components, the highest coverage spectrum measured after deposition at T=80 K (Fig. 1(c)) shows an additional shoulder (C) at about 284.7 eV. It is worth underlining that while the D component is quite broad with a FWHM of about 0.6 eV, the M peak is narrower and displays a shoulder at lower binding energy. This suggests that, for the highest coverage, not less than four non-equivalent carbon species, *i.e.* existing in a slightly different local environment, have been produced after deposition.

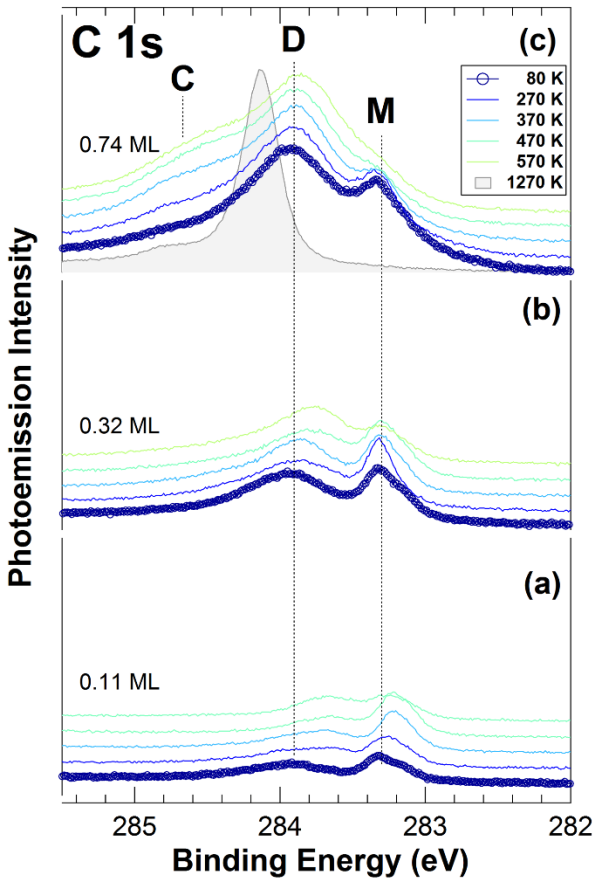

Figure 1. C 1s spectra after deposition (T=80 K) of (a) 0.11 ML, (b) 0.32 ML and (c) 0.74 ML of carbon (dotted blue lines), and after subsequent annealing to increasing temperatures (thin lines). Spectra are measured at hυ =400 eV and at normal emission. The grey filled spectrum corresponds to graphene island formation. The binding energy positions of carbon monomers (M), dimers (D) and larger clusters (C) are indicated.

The annealing process induces clear modifications in the C 1s core level lineshape, the major effects being (i) a reduction of the M component and (ii) an increase and a shift to lower binding energies of the D and C components. The reasons of the C 1s spectral changes can be attributed to the modification of the adsorption configurations, the density of the different surface species and to the formation of different carbon clusters, as will be discussed below.

For the high carbon coverage deposition we have also included the spectrum obtained after annealing the surface to 1270 K, a process that is known to produce large graphene islands[36]. The binding energy of the main peak at 284.1 eV is in agreement with previous findings[37-39],

while the shoulder at about 284.6 eV could be assigned to carbon atoms in defective configurations[40].

In order to obtain further information about the local carbon atom configuration, along with the variations of the electronic structure of substrate Ir atoms, we also acquired Ir $4f_{7/2}$ core level spectra. They are displayed in Fig. 2, which shows a series of Ir $4f_{7/2}$ spectra corresponding to different carbon coverage, from the clean surface (bottom), to the highest C coverage structure (top). As already reported[24], the spectrum corresponding to the clean Ir(111) surface (Fig. 2(a)) can be described by two peaks: the higher binding energy component, at 60.85 eV, originates from subsurface and deeper layers, while the lower binding energy (BE) peak S_0, shifted by −550±10 meV with respect to the bulk peak, originates from the topmost Ir atoms. A two component analysis gives best fit values for the Γ, α and G parameters respectively of 0.25 eV, 0.10, and 0.10 eV for the bulk, and 0.25 eV, 0.17, and 0.12 eV for the surface component.

We found that all the spectra for the different C coverages can be properly fitted by adding new surface components, as revealed by the low fitting residuals and by the chi-square analysis. In order to evaluate the intensity and CLSs of the different surface components induced by the proximity of C atoms, we performed a fit of the Ir $4f_{7/2}$ spectra for each of the C doses. The fit was performed by fixing the BE position and the lineshape parameters of the bulk and S_0 peak, while all the surface components were constrained to have the same lineshape found for the clean surface component S_0.

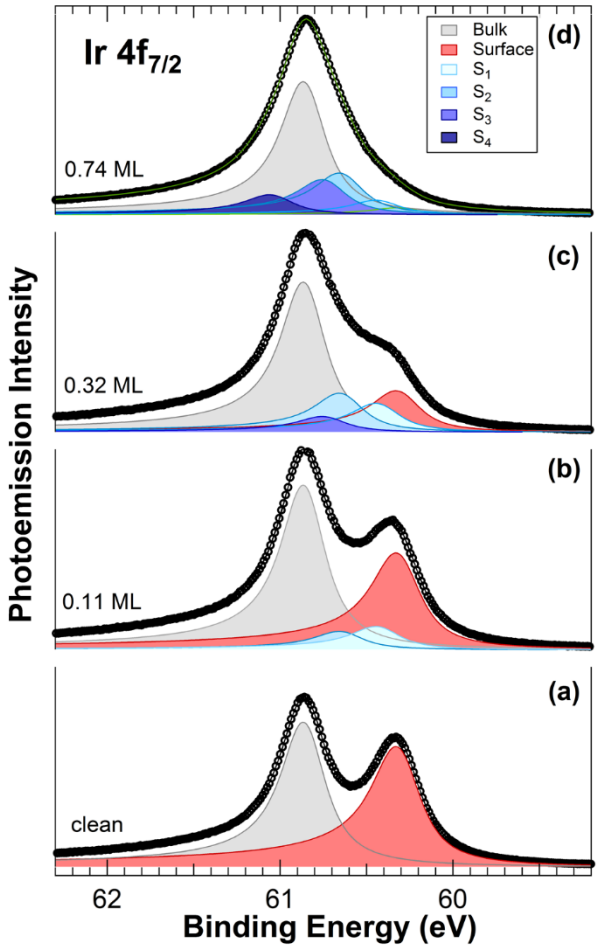

Figure 2. Ir $4f_{7/2}$ core level spectra corresponding to the Ir(111) surface after cleaning (bottom) and after deposition at 80 K of different carbon coverages. Deconvoluted bulk (grey) and Surface (red) components are shown together with carbon-induced surface core level shifted peaks (S_1-S_4). The spectra were measured at T=80 K, for hυ =200 eV and at normal emission.

The low carbon coverage of 0.11 ML (Fig. 2(b)) leads to the appearance of two additional core level shifted components, S_1 and S_2, shifted by −430 ± 20 and −220 ± 20 meV with respect to the bulk component, while the original S_0 surface peak intensity decreases. Upon increasing the C coverage (0.32 ML spectrum, Fig. 2(c)) we observe a further decrease of S_0, accompanied by the growth of a third carbon-induced surface component, S_3, at a binding energy close to the BE of the bulk component (−120 ± 20 meV). Finally, in order to properly fit the 0.74 ML spectrum (Fig. 2(d)), a new component, with a positive surface CLSs (+180 ± 20 meV), needs

to be included. Although the different components cannot be unambiguously assigned to specific cluster configurations, the trend observed can be explained as due to a progressive increase in the coordination of the first-layer Ir atoms with C atoms: according to what we measured for several atomic adsorbates on a variety of transition metal surfaces[41-48], surface core level shifted components are linked to surface Ir atoms forming one (S_1), two (S_2) or even larger (S_{3-4}) number of bonds with adsorbates. For our system, this model is over simplified, as it only considers the number of C atoms coordinated with Ir atoms, while possible differences in the local geometry are not taken into account. For example, within this approach the adsorption of two C monomers next to each other results in the production of the same surface CLS as for a single carbon dimer. Nevertheless, from a qualitative point of view, the results of the Ir 4f7/2 core level analysis suggest that the surface gets increasingly occupied by C species in such a way that at a coverage of 0.74 ML the density of pristine first-layer Ir atoms not coordinated with adsorbates is negligible. This indicates that at the highest coverage the system is formed by a large number of different and contiguous C clusters placed in non-equivalent configurations. On the basis of these results we decided to focus the C 1s core level analysis only on the two low coverage systems we have prepared, namely 0.11 and 0.32 ML. For our system, this model is over-simplified, as it only considers the number of C atoms coordinated with Ir atoms, while possible differences in the local geometry are not taken into account. For example, within this approach the adsorption of two C monomers next to each other would result in the same surface CLS as for a single carbon dimer. Besides coordination, C atoms can occupy a large variety of slightly different positions relative to the Ir surface, resulting in a broader distribution of binding energies. For these reasons, it is not possible to identify in an unambiguous way a relationship between surface core level shifted components and non-equivalent Ir atoms.

4.2 Theoretical results

To explain the origin of the different components observed in the C 1s photoemission spectra we performed DFT calculations by investigating the preferred adsorption sites/configurations and formation energies of carbon clusters of different sizes on Ir(111), ranging from monomers (C_1) to pentamers (C_5). The results are reported in Figure 3. For all these clusters (C_1-C_5) we also calculated the C 1s CLS of each of their atomic constituents, which are reported in Table 1.

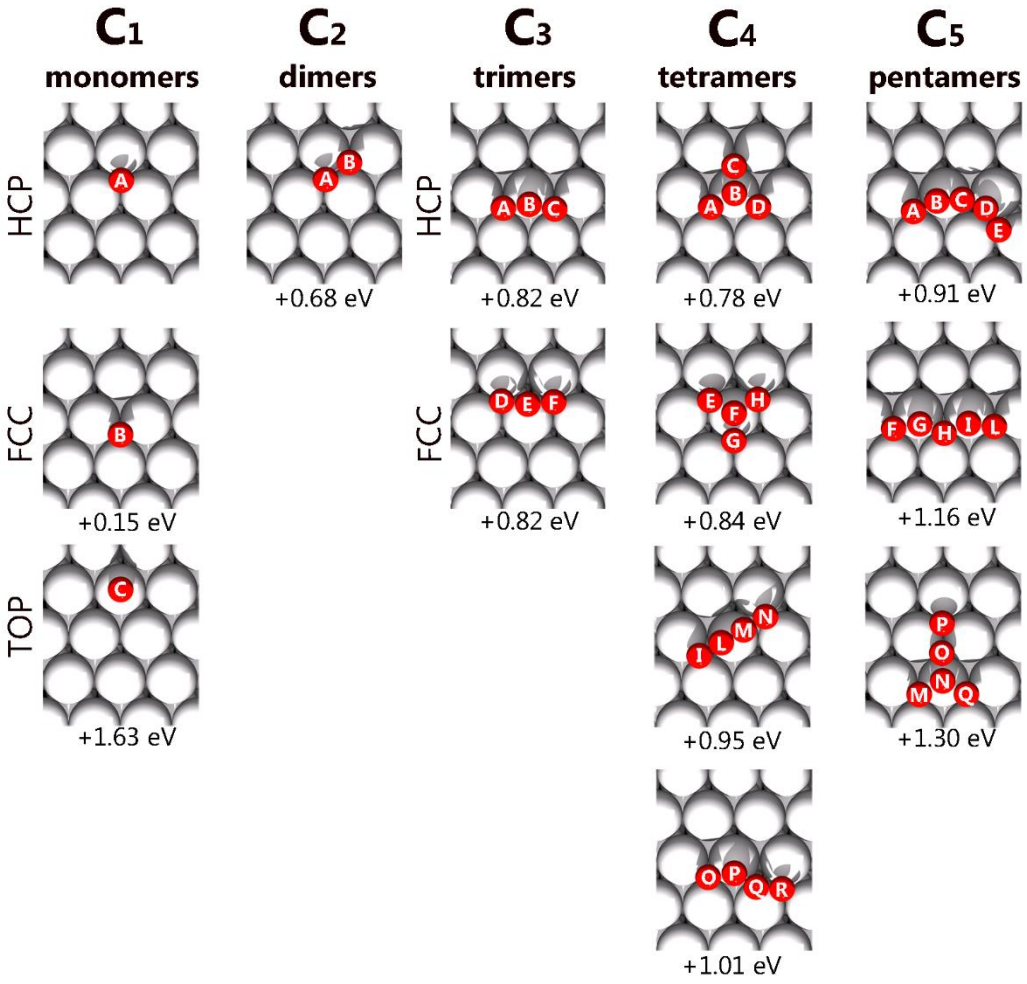

Figure 3. Stable configurations of the carbon species adsorbed onto the Ir(111) surface. The formation energy of each species is also included. Non-equivalent carbon atoms are labelled with different letters.

In particular, carbon adatoms (C_1) can adsorb in three configurations: top, three-fold hollow (either FCC or HCP), or bridge that however is energetically unstable and relaxes to the hollow site. The most favorable adsorption site is HCP, with an energy gain of 0.15 eV with respect to the FCC, while the top site is considerably less stable. By referring the binding energy scale to the value of the calculated C 1s core electron binding energy for the C monomers in HCP ($C_{1,A}$) we find shifts of -0.12 ($C_{1,B}$) and +0.11 ($C_{1,C}$) eV for monomers in FCC and top sites, respectively.

	monomers	dimers	trimers	tetramers	pentamers
A	0	+0.650	+0.920	+0.727	+0.745
B	-0.120	+0.510	+0.370	+0.152	+0.351
C	+0.110		+0.920	+1.022	+1.486
D			+0.780	+0.543	+0.310
E			+0.190	+0.609	+0.559
F			+0.780	+1.514	+0.680
G				+0.614	+1.908
H				+0.614	+1.270
I				+0.773	+0.675
L				+1.488	+0.681
M				+0.773	+0.828
N				+0.773	+0.366
O				+0.890	+0.343
P				+0.679	+0.164
Q				+0.651	+0.797
R				+0.972	

Table 1. C 1s Core Level Shifts of C monomers in different adsorption sites and each C atom in small clusters with different geometry.

Carbon dimers (C_2) are only stable when two C atoms (with the C-C bond length of 1.38 Å) are placed in FCC and HCP adsorption sites: since the two carbon atoms are geometrically non-equivalent, the C1s BE is shifted by +0.51 and +0.65 eV, respectively, for the C atoms that locally occupy the FCC ($C_{2,A}$) and HCP ($C_{2,B}$) configurations.

Finally, the most stable adsorption sites for C trimers (C_3) are those with an almost linear atomic arrangement, whose central atoms are placed close to either FCC ($C_{3,B}$) or HCP ($C_{3,E}$) sites, but slightly out of axis, being displaced towards the nearest-neighbor first layer Ir atom. The two C atoms placed at the edges in each trimer are instead both in HCP ($C_{3,A}$ and $C_{3,C}$) or FCC sites ($C_{3,D}$ and $C_{3,F}$), respectively. The two adsorption configurations are energetically degenerate. The corresponding CLS for both types of trimers are positive (see Table 1), with a negligible difference between the values calculated for the side atoms of each configuration: these values are a further indication of the high-symmetry in C_3 cluster configurations.

It is clear from Fig. 3 that C_1 monomers in FCC and HCP sites are energetically more favorable with respect to dimers and trimers, in agreement with previous experimental and theoretical findings[6,12]. This is also valid for the formation energies of clusters made of 4 (C_4) and 5 carbon (C_5) atoms, which are positive, as shown in Fig. 3 (right side). As a consequence we expect the density of monomers on Ir(111) terraces during any process which produce only C1 adatoms (such as high-temperature ethylene molecular dissociation[49]), to be much larger than the density of $C_{2\text{-}5}$ clusters.

This conclusion is also supported by detailed calculations of formation energies of various carbon clusters on the Ir(111) surface at zero and non-zero temperatures[50]; it was also found in this study that significant energy barriers (over 1 eV) are to overcome in order to form larger clusters by successfully adding monomers.

4.3 Analysis of low temperature C 1s core level spectra

On the basis of the theoretical results we performed the analysis of the C 1s spectra (Fig. 4). The search for the optimal parameters in terms of C 1s lineshape and CLSs was performed in the multi-dimensional parameter space by adopting a strategy to understand correlation effects between parameters that has already been successfully used in previous works[51]. In particular, we analyzed the χ^2 contour plots, in which the evolution of the χ^2 is mapped while two fitting coefficients are simultaneously varied, and evaluated the presence of deep and localized minima in the phase space diagram. The values obtained for the other free fitting parameters were plotted in parallel, as a function of the same coordinates. This procedure allowed us to estimate the error bar affecting the values found for the fitting parameters: for each contour plot, we selected the region were the χ^2 lay within 10% from its minimum and calculated the corresponding variation in the fitting coefficients.

We started our analysis on the data acquired for the lowest coverage (see Fig. 4(a)), where we expected to find only a few C species on the surface, namely single C_1 adatoms or very small clusters, such as C_2 dimers and C_3 trimers. The calculated C 1s CLSs suggest that the C monomers are the surface species with the lowest C 1s BEs, and therefore could originate the narrow spectral components in the range between 283.5 and 283 eV.

We decided to align the calculated and the experimental binding energy scale in such a way that the highest intensity component at about 283.35 eV corresponds to the most favorable configuration, *i.e.* the C_1 species in HCP sites ($C_{1,A}$), and expressed the BE of all other components in terms of their separation from this one. This is a necessary step since DFT only provide relative BE shifts.

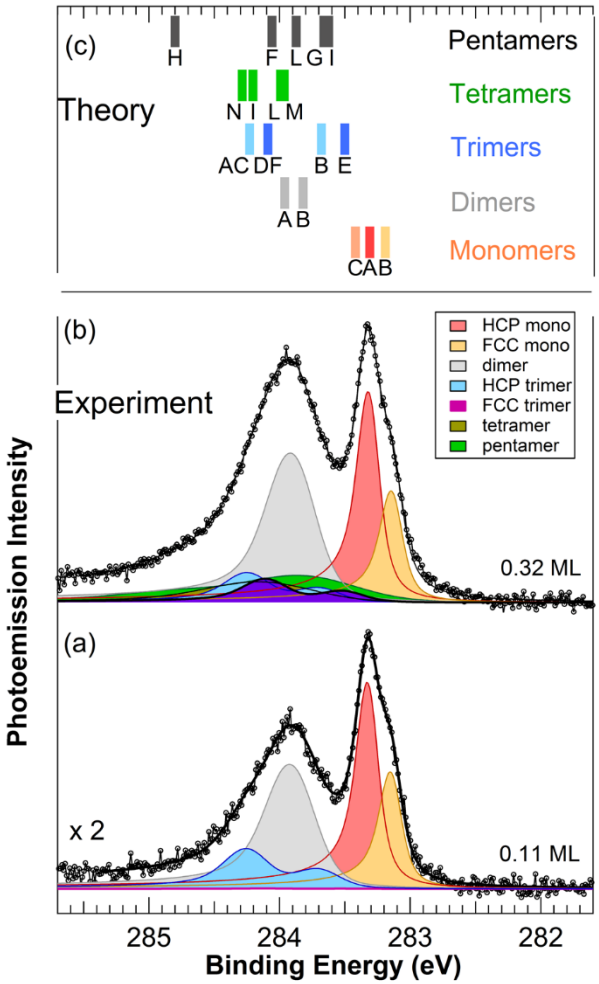

Figure 4. Calculated C1s core level binding energies (top) and C 1s spectra after deposition of 0.11 ML (bottom) and 0.32 ML (middle) carbon coverage (T= 80 K) together with the deconvoluted components of each carbon species. Spectra are measured at hυ =400 eV and at normal emission.

In the first step of our analysis, we determined the lineshape of the components originating from the M double peak. This was done by analyzing the region of minimum χ^2 of the fit while ranging step by step the Gaussian parameter G_1 around an initial guess and the CLS around the theoretically calculated value. We repeated this procedure twice, allowing the Lorentzian L and the asymmetry parameter α, one at a time, to relax for each point in the parameter space explored. Using this procedure, we found a CLS of -170 ± 20 meV between monomers adsorbed in HCP and FCC (see Fig. 5(a)), which is in quite good agreement with the theoretically calculated value of -120 meV.

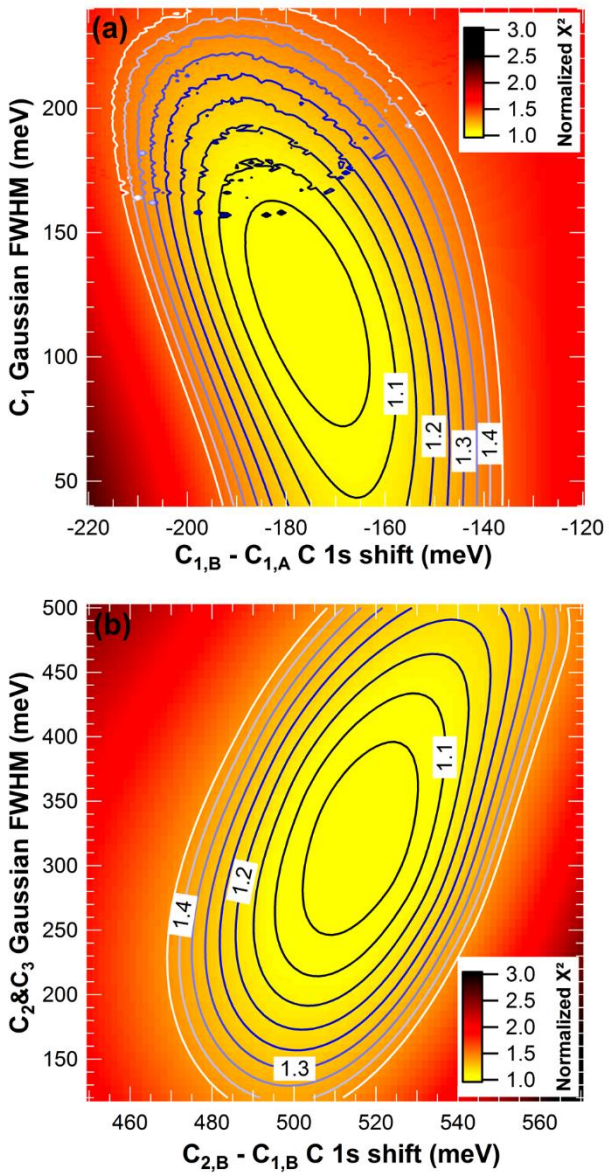

Figure 5. Two-dimensional contour plots of the chi-square maps referred to the fit of C 1s core-level spectrum (0.11 ML carbon coverage) measured at hυ=400 eV and at normal emission. The plots show the normalized chi square χ2 / χ2MIN as a function of (a) Gaussian FWHM of monomers C1 versus C 1s core level shift between monomers adsorbed in FCC and HCP three-fold sites and (b) Gaussian FWHM of dimers C2 and trimers C3 versus core level shift between dimers C2 and monomers adsorbed in HCP three-fold sites.

Following this, we repeated this procedure to determine the lineshape and CLS for the highest binding energy photoemission components where, according to the theoretical CLSs in Fig. 4(c), the spectral intensity is most probably originated from the presence of dimers and trimers. We fixed their DS lineshape parameters (L and α) to those already found for the low binding

energy component. A further constraint was used for the intensities I of the different carbon species, by keeping $I(C_{2,a})=I(C_{2,b})$, $I(C_{3,a})=I(C_{3,b})=I(C_{3,c})$ and $I(C_{3,d})=I(C_{3,e})=I(C_{3,f})$.

Moreover, since the deconvolution of these components cannot be easily performed due to their small CLSs (as pointed out in the calculations), we decided to fix their relative shifts to the theoretically calculated values, refining the BE shift between all of them and the reference (the monomers in HCP sites), and to keep the lineshape equal for all these components, *i.e.* we used a single parameter for the Gaussian $G_{2,3}$ of all C_2 and C_3 clusters photoemission components. We then monitored the evolution of the χ^2 as a function of this Gaussian FWHM G and of CLS, with respect to the HCP monomer. The image plot of the χ^2 minimum, reported in Fig. 5(b), reveals that the CLS experimental results are consistent with the theoretically calculated values to within 50 meV. The best lineshape parameters we found are L=120 meV, α=0.117, while the Gaussian values were G_1=120 and $G_{2,3}$=316 meV, for monomers and dimers/trimers, respectively. The deconvoluted photoemission components as obtained from the fit are shown in different colors in Fig. 4, where each curve represents the sum of the contributions from all the atoms in a cluster. Since the FWHM values of the individual components are at times larger than the theoretically calculated BE splitting between these components, the individual components generating the spectrum of each kind of cluster cannot always be resolved. This is particularly true for the components arising from dimers and trimers, where the Gaussian component has been found to be larger than in the case of C monomers, because of enhanced vibrational broadening, as found for diatomic molecules[52].

The fitting residual, which shows no appreciable modulations, suggests that this system is composed by clusters formed by at most three atoms. The intensity of the different components (see Table 2) provides the coverage of monomers (in HCP and FCC adsorption sites), dimers and trimers.

It is interesting to note that the intensity of the monomer component slightly increases with increasing the annealing temperature, in agreement with the theoretical prediction that monomers are more thermodynamically stable.

The same procedure was applied to the C 1s spectrum acquired at higher coverage (0.32 ML), shown in Fig. 4(b). However, in this case it was necessary to take into account also larger clusters, namely tetramers and pentamers, to correctly describe the experimental data. This was particularly important for the high binding energy shoulder at about 284.7 eV, that according to the DFT calculations can only be justified by assuming that C_4 and C_5 species are present on the surface. The first step in the analysis of this spectrum was to introduce only one type of tetramer or pentamer at a time with a free Gaussian $G_{4,5}$ component, still keeping L and α at the value found for the lower coverage spectrum. The best agreement was achieved by including tetramers formed by $C_{4,N}$, $C_{4,I}$, $C_{4,L}$, $C_{4,M}$, reported in Fig. 3. Only in the final step we added a new species in order to minimize the χ^2: pentamers with C atoms arranged in a linear fashion (top structure in Fig. 3 under Pentamers) were those providing the lowest χ^2.

While it is not possible to draw a clear-cut picture about the concentration of the different C_4 and C_5 species, our results unambiguously show that the 0.32 ML coverage structure cannot be described by including just monomers, dimers and trimers, as was the case for the lowest coverage spectrum. Owing to this behavior and to the results of the Ir $4f_{7/2}$ analysis described above, we did not make any fitting of the 0.77 ML spectrum, shown in Fig. 1. Nevertheless, this spectrum is consistent with our findings, as it displays an increased spectral intensity towards higher BEs, were we expect to have, besides the C dimers at 284.8 eV, also larger C clusters.

4.4 Origin of monomers and dimers

The analysis of the coverage of the different species obtained after low temperature deposition provides an interesting information about the growth of graphene. As reported in Table 2 the deposition of 0.11 ML at T=80 K results in the formation of 0.037, 0.021 and 0.040 ML of monomers HCP, monomers FCC and dimers, respectively, and with 0.016 ML of trimers. We compared these results with those obtained using a random deposition model, in which C atoms are randomly distributed on the (111) surface, with the possibility of occupying with equal probability HCP and FCC three-fold sites and with the assumption that, when sitting in neighboring three-fold sites, they form a dimer. Besides the experimentally observed strong preference for the occupation of HCP sites in comparison with that for FCC sites, which is in agreement with our theoretical findings, the main difference between experimental and theoretical results is found in the relative populations of dimers and monomers. In fact, the experimental occupation of C atoms in the dimer configuration (35 %) is much larger than the value obtained with the random deposition model calculation (13.5 %).

	C_1-HCP	**C_1-FCC**	**C_2**	**C_3-HCP**	**C_3-FCC**	**others**	**total**
experiment	0.037 (32.5%)	0.021 (18.5%)	0.040 (35%)	0.016 (14%)	0	0	**0.114**
random deposition model	0.0478 (42%)	0.0478 (42%)	0.0154 (13.5%)	0.0012 (1%)	0.0012 (1%)	0.0006 (0.5%)	**0.114**

Table 2. Coverage of carbon monomers and clusters measured on the surface and obtained from a random deposition model.

This discrepancy could be explained as due to (i) diffusion of energetic C adatoms on the surface (that effect was not included in our random deposition model) with subsequent

formation of dimers already at low temperature or (ii) deposition of C dimers on the surface originating directly from the graphite rod in the sublimation process. However, the first hypothesis can be disregarded since C dimers are energetically unflavored with respect to C monomers by 0.68 eV (Fig. 3 and [49]).

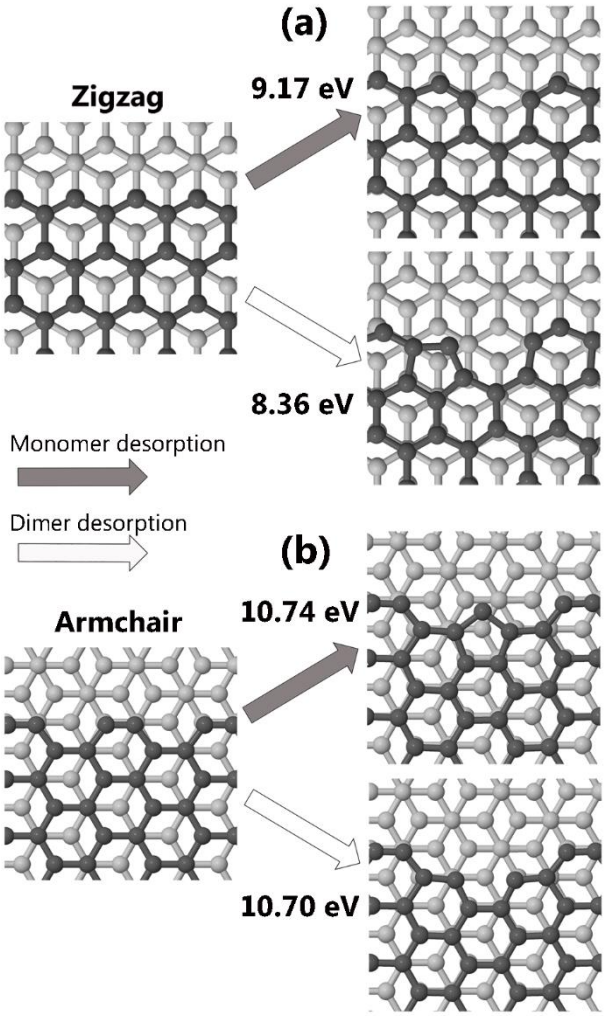

Figure 6. Initial (left) and final (right) geometrical configurations in NEB calculations for the sublimation of carbon monomers (dark arrow) and dimers (white arrow) from zigzag (a) and armchair (b) graphite edges. Corresponding energy barriers are also reported.

In order to support the second hypothesis about the sublimation of different C species, we have performed NEB monomer and dimer detachment calculations on graphite with different

initial state geometries. In particular, we considered a graphite surface showing zig-zag (Fig. 6(a)) or armchair monoatomic step edges (Fig. 6(b)), both of which have been experimentally found in scanning tunneling microscopy measurements on highly oriented pyrolytic graphite[53]. In these defective sites the C atoms have to break a smaller number of bonds with respect to the sp_2 inner C atoms configuration. For both edge configurations we calculated the energy barrier of the processes in which either a monomer or dimer was removed. It is clear that the detachment mechanism showing the lowest barrier ($E_{barrier}$= 8.36 eV) is the removal of a dimer from a zig-zag edge.

These results are in agreement with what was observed experimentally, for instance in high temperature transmission electron microscopy measurements[54]. While we believe that several others local defective configurations can be present on the graphite rod surface, our results suggest that dimers can be directly deposited by means of sublimation from graphite, which therefore represents an ideal source for the study of their properties.

4.5 Graphene growth at high-temperature by means of chemical vapor deposition

In order to obtain information about the different C species which are present during the CVD growth, we exploited the snapshot fast-XPS operation mode, in which the evolution of the C 1s core level was monitored in real time while dosing ethylene at T=820 K from a supersonic beam of C_2H_4 molecules.

Figure 7(a) shows a two-dimensional plot of the time-lapsed C 1s spectra, with the photoemission intensity being represented as a density plot by a color scale, ranging from low (black) to high (white). As previously found with temperature programmed growth experiments[37], the C 1s intensity is centered at around 284.1 eV and can be ascribed to C atoms forming C nanodomes and small graphene islands growing with a very high surface density. The variation of the BE is due to the modified coupling of the C layers with the Ir substrate

with increasing size of the nucleating graphene islands. The most interesting feature which is dominant at the beginning of the growth process is a low binding energy C 1s component centered at 283.35 eV. Indeed (as shown by the selected uptake spectra in Fig. 7(b)), while for large exposure the C 1s spectrum can be fitted with just three components[37] - one due to the atoms at the center of the clusters, the others either to atoms at the periphery of the Gr clusters bound to 2 C atoms (BE=283.7 eV), or to C atoms directly bound to the periphery and connected to 3 C atoms (BE=284.4 eV) - in the very low coverage range a small component has to be additionally included at the same BE found for the monomer species to obtain a proper fit of the experimental data. This peak, growing in intensity up to a maximum coverage of 0.08 ML, slowly disappears with increasing ethylene exposure (Fig. 7(c) and (d)). This behavior, characterized by an initial increase of the C adatoms which then drops when Gr nucleation starts, has already been observed by low energy electron reflectivity measurements during Gr growth on Ir(111)[4]. In particular, McCarty *et al*. observed during GR growth on Ir(111) at 1100 K a maximum C adatom concentration of 0.032 ML, which is qualitatively comparable to the value we obtained. The differences can be explained for example in terms of the different growth conditions, such as different C_2H_4 pressure and substrate temperature: an analogous behavior was actually observed for example in the case of Ru(0001), where the C adatom concentration at which graphene nucleation starts is higher at lower temperature[55]. The concentration observed on Ru(0001) at the same growth temperature, on the other hand, is significantly smaller than what we measured on Ir(111): this fact can be explained by the weaker C-metal interaction, which is known to favor the dissolution of C atoms into the bulk and might therefore reduce the equilibrium concentration of adsorbed C monomers – as shown by the higher enthalpy of formation of C monomers on the Ir(111) surface. Bulk dissolution upon annealing and subsequent segregation during cooling is in fact an effective method for

growing Gr on metal surfaces which show a strong interaction with C such as Ni[56], Re[57,58] and Pd[59].

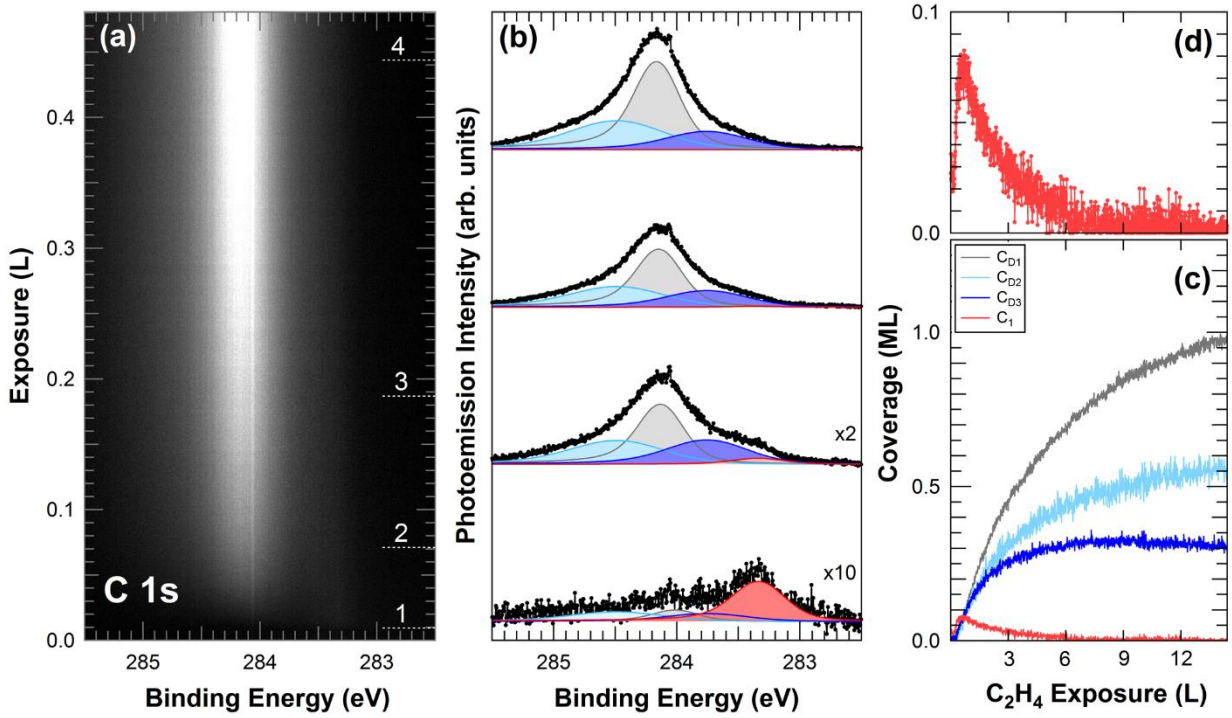

Figure 7. Evolution of C 1s spectra during ethylene uptake at T= 820 K (hυ=400 eV). (a) Coverage-dependent C 1s core-level spectra (about 1250 spectra) shown as a two-dimensional intensity plot. (b) Deconvoluted C 1s components from selected spectra of the uptake (numbered from 1 to 4 in (a)). (c) Evolution of the C coverage of the different species: C atoms at the center of the graphene clusters (grey), atoms at the periphery of the clusters bound to 2 C atoms (light blue), and sp_2 C atoms directly bound to the periphery of the clusters (blue). The component due to C monomer is shown in red. (d) Evolution of monomers coverage.

Besides the use of C 1s BE as a fingerprint of the presence of monomers on the surface, a further proof of the assignment of the low binding energy component in Fig. 7(b) to monomers comes from the plot of the monomers coverage as a function of the carbon coverage in the graphene nanodomes (see Fig. 8), which can be simply calculated by summing up the

intensities of three components which are assigned to different C species (C_{D1}, C_{D2} and C_{D3} in Fig. 7(c)) forming the small graphene flakes. The plot clearly shows that above a critical coverage the monomers coverage diminishes with a linear behavior, which is consistent with the density of monomers depending on the free surface area, i.e. the portion of the Ir surface which is not covered by (or adjacent to) carbon nanodomes. It is therefore the portion of clean Ir(111) surface which determines the density of monomers diffusing on the surface before attaching to the edges of the nanodomes. These results suggest therefore that a C adatom lattice gas is present also at the early stage of graphene growth on Ir(111) by means of C_2H_4 CVD.

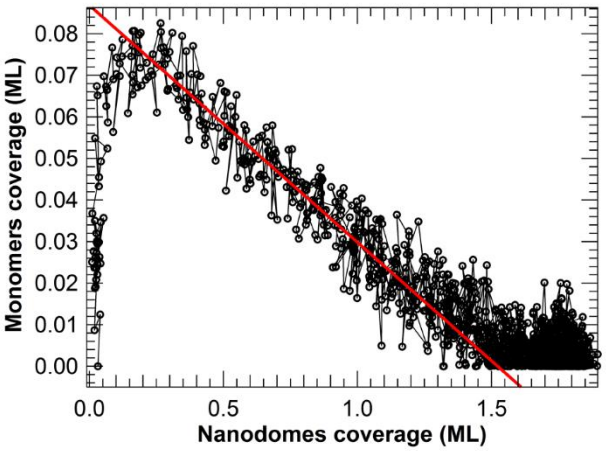

Figure 8. Evolution of the population of C monomers versus the C nanodomes coverage corresponding to small graphene clusters during ethylene uptake at T=820 K.

5. Conclusions

By combing experiment and theory we have shown that the C 1s core level component at BE=283.35 eV can be used as a fingerprint for C monomers in two systems where either small C clusters (dimers, trimers, etc.) or Gr nanoislands are present together.

In particular, we have shown that the low temperature MBE of carbon atoms using a solid-state graphite source results in a distribution of C clusters whose sizes depend on the surface density of carbon atoms and that high resolution core level spectroscopy can provide quantitative results on the relative concentration of the different species and, in the case of monomers, even on their adsorption sites. These measurements allowed us to conclude that which species are present on the surface is not only determined by their interactions, but is strongly dependent on the dynamics by which they are generated by the C source. In particular, we find that C dimers, alongside the monomers, are also present in the beam and hence directly deposited on the surface.

Based on the interpretation of the low temperature data, the presence of a carbon adatom lattice gas during ethylene uptake performed at high temperature (T=820 K) was demonstrated, in particular during at the early stages of Gr growth, when a significant density of monomers (C 1s component at 283.35 eV) was detected already before the nucleation process started. We believe therefore that C 1s high resolution core level spectroscopy can provide very useful information about the role of monomers and dimers during the growth of graphene on different metal surfaces.

AUTHOR INFORMATION

Corresponding Author

* Alessandro Baraldi, baraldi@elettra.eu, +39 040 3758719

ACKNOWLEDGMENT

We acknowledge the financial support from the University of Trieste through the program ‘‘Finanziamento di Ateneo per progetti di ricerca scientifica - FRA 2014’’.

REFERENCES

(1) Wu, P.; Zhang, W.; Li, Z.; Yang, J. Mechanisms of Graphene Growth on Metal Surfaces: Theoretical Perspectives. *Small* **2014**, *10*, 2136–2150.

(2) Tetlow, H.; Posthuma de Boer, J.; Ford, I. J.; Vvedensky, D. D.; Coraux, J.; Kantorovich, L. Growth of Epitaxial Graphene: Theory and Experiment. *Phys. Rep.* **2014**, *542*, 195–295.

(3) Seah, C.-M.; Chai, S.-P.; Mohamed, A. R. Mechanisms of Graphene Growth by Chemical Vapour Deposition on Transition Metals. *Carbon* **2014**, *70*, 1-21.

(4) Loginova, E.; Bartelt, N. C.; Feibelman, P. J.; McCarty, K. F. Factors Influencing Graphene Growth on Metal Surfaces. *New J. Phys.* **2009**, *11*, 063046.

(5) Loginova, E.; Bartelt, N. C.; Feibelman, P. J.; McCarty, K. F. Evidence for Graphene Growth by C Cluster Attachment. *New J. Phys.* **2008**, 1*0*, 093026.

(6) Wu, P.; Jiang, H.; Zhang, W.; Li, Z.; Hou, Z.; Yang, J. Lattice Mismatch Induced Nonlinear Growth of Graphene. *J. Am. Chem. Soc.* **2012**, *134*, 6045-6051.

(7) Yazyev, O. V.; Chen, Y. P. Polycrystalline Graphene and Other Two-Dimensional Materials. *Nat. Nanotech.* **2014**, *9*, 755–767.

(8) Riikonen, S.; Krasheninnikov, A. V.; Halonen, L.; Nieminen, R. M. The Role of Stable and Mobile Carbon Adspecies in Copper-Promoted Graphene Growth. *J. Phys. Chem. C* **2012**, *116*, 5802−5809.

(9) Niu, T.; Zhou, M.; Zhang, J.; Feng, Y.; Chen, W. Growth Intermediates for CVD Graphene on Cu(111): Carbon Clusters and Defective Graphene. *J. Am. Chem. Soc.* **2013**, *135*, 8409-8414.

(10) Wu, P.; Zhang, Y.; Cui, P.; Li, Z.; Yang, J.; Zhang, Z. Carbon Dimers as the Dominant Feeding Species in Epitaxial Growth and Morphological Phase Transition of Graphene on Different Cu Substrates. *Phys. Rev. Lett.* **2015**, *114*, 216102.

(11) Zhong, L.; Li, J.; Li, Y.; Lu, H.; Du, H.; Gan, L.; Xu, C.; Chiang, S. W.; Kang, F. Unraveling the Influence of Metal Substrates on Graphene Nucleation From First-Principles Study. *J. Phys. Chem. C* **2016**, *120*, 23239−23245.

(12) Chen, H.; Zhu, W.; Zhang, Z. Contrasting Behavior of Carbon Nucleation in the Initial Stages of Graphene Epitaxial Growth on Stepped Metal Surfaces. *Phys. Rev. Lett.* **2010**, *104*, 186101.

(13) Gao, M.; Zhang, Y.-F.; Huang, L.; Pan, Y.; Wang, Y.; Ding, F.; Lin, Y.; Du, S.-X.; Gao, H.-J. Unveiling Carbon Dimers and Their Chains as Precursor of Graphene Growth on Ru(0001). *Appl. Phys. Lett.* **2016**, *109*, 131604.

(14) Xu, L.; Jin, Y.; Wu, Z.; Yuan, Q.; Jiang, Z.; Ma, Y.; Huang, W. Transformation of Carbon Monomers and Dimers to Graphene Islands on Co(0001): Thermodynamics and Kinetics. *J. Phys. Chem. C* **2013**, *117*, 2952-2958.

(15) Xu, L.; Ma, Y.; Wu, Z.; Chen, B.; Yuan, Q.; Huang, W. A Photoemission Study of Ethylene Decomposition on a Co(0001) Surface: Formation of Different Types of Carbon Species. *J. Phys. Chem. C* **2012**, *116*, 4167−4174.

(16) Li, J.; Croiset, E.; Ricardez-Sandoval, L. Carbon Clusters on the Ni(111) Surface: a Density Functional Theory Study. *Phys. Chem. Chem. Phys.* **2014**, *16*, 2954-2961.

(17) Gao, J.; Yuan, Q.; Hu, H.; Zhao, J.; Ding, F. Formation of Carbon Clusters in the Initial Stage of Chemical Vapor Deposition Graphene Growth on Ni(111) Surface. *J. Phys. Chem. C* **2011**, *115*, 17695–17703.

(18) Fu, Z.; Zhang, Y.; Yang, Z. Growth Mechanism and Controllable Synthesis of Graphene on Cu–Ni Alloy Surface in the Initial Growth Stages. *Phys. Lett. A* **2015**, *379*, 1361-1365.

(19) Page, A. J.; Ding, F.; Irle, S.; Morokuma, K. Insights into Carbon Nanotube and Graphene Formation Mechanisms from Molecular Simulations: A Review. *Rep. Prog. Phys.* **2015**, *78*, 036501.

(20) Long, N. J.; Williams, C. K. Metal Alkynyl σ Complexes: Synthesis and Materials. *Angew. Chem. Int. Ed.* **2003**, *42*, 2586-2617.

(21) Yam, V. W.-W. Molecular Design of Transition Metal Alkynyl Complexes as Building Blocks for Luminescent Metal-Based Materials: Structural and Photophysical Aspects. *Acc. Chem. Res.* **2002**, *35*, 555-563.

(22) Hernández-Rodríguez, I.; García, J. M.; Martín-Gago, J. A.; de Andrés, P. L.; Méndez, J. Graphene Growth on Pt(111) and Au(111) Using a MBE Carbon Solid-Source. *Diamond Relat. Mater.* **2015**, *57*, 58-62.

(23) Lippert, G.; Dąbrowski, J.; Schroeder, T.; Schubert, M. A.; Yamamoto, Y.; Herziger, F.; Maultzsch, J.; Baringhaus, J.; Tegenkamp, C.; Asensio, M. C.; *et al.* Graphene Grown on Ge(001) From Atomic Source. *Carbon* **2014**, *75*, 104-112.

(24) Bianchi, M.; Cassese, D.; Cavallin, A.; Comin, R.; Orlando, F.; Postregna, L.; Golfetto, E.; Lizzit, S.; Baraldi, A. Surface Core Level Shifts of Clean and Oxygen Covered Ir(111). *New J. Phys.* **2009**, *11*, 063002.

(25) Baraldi, A.; Rumiz, L.; Moretuzzo, M.; Barnaba, M.; Comelli, G.; Lizzit, S.; Paolucci, G.; Rosei, R.; Buatier de Mongeot, F.; Valbusa, U. A Supersonic Molecular Beam for Gas–

Surface Interaction Studies with Synchrotron Radiation. *J. Vac. Sci. Technol. A* **2002**, *20*, 683-687.

(26) Doniach, S.; Šunjić, M. Many-Electron Singularity in X-Ray Photoemission and X-Ray Line Spectra from Metals. *J. Phys. C: Solid State Phys.* **1970**, *3*, 285-291.

(27) Hutter, J.; Iannuzzi, M.; Schiffmann, F.; VandeVondele, J. CP2K: Atomistic Simulations of Condensed Matter Systems. *Wiley Interdiscip. Rev.: Comput. Mol. Sci.* **2014**, *4*, 15-25.

(28) Perdew, J. P.; Burke, K.; Ernzerhof, M. Generalized Gradient Approximation Made Simple. *Phys. Rev. Lett.* **1996**, *77*, 3865.

(29) Goedecker, S.; Teter, M.; Hutter, J. Separable Dual-Space Gaussian Pseudopotentials. *Phys. Rev. B* **1996**, *54*, 1703.

(30) VandeVondele, J.; Hutter, J. Gaussian Basis Sets for Accurate Calculations on Molecular Systems in Gas and Condensed Phases. *J. Chem. Phys.* **2007**, *127*, 114105.

(31) Grimme, S.; Antony, J.; Ehrlich, S.; Krieg, H. A Consistent and Accurate Ab Initio Parametrization of Density Functional Dispersion Correction (DFT-D) for the 94 Elements H-Pu. *J. Chem. Phys.* **2010**, *132*, 154104.

(32) Kresse, G.; Furthmüller, J. Efficiency of Ab-Initio Total Energy Calculations for Metals and Semiconductors Using a Plane-Wave Basis Set. *Comp. Mat. Sci.* **1996**, *6*, 15-50.

(33) Kresse, G.; Furthmüller, J. Efficient Iterative Schemes for Ab Initio Total-Energy Calculations Using a Plane-Wave Basis Set. *Phys. Rev. B* **1996**, *54*, 11169-11186.

(34) Kresse, G.; Hafner, J. Ab Initio Molecular Dynamics for Liquid Metals. *Phys. Rev. B* **1993**, *47*, 558-561.

(35) Köhler, L.; Kresse, G. Density Functional Study of CO on Rh(111). *Phys. Rev. B* **2004**, *70*, 165405.

(36) Coraux, J.; N'Diaye, A. T.; Engler, M.; Busse, C.; Wall, D.; Buckanie, N.; Meyer zu Heringdorf, F.-J.; van Gastel, R.; Poelsema, B.; Michely, T. Growth of Graphene on Ir(111). *New J. Phys.* **2009**, *11*, 023006.

(37) Lacovig, P.; Pozzo, M.; Alfè, D.; Vilmercati, P.; Baraldi, A.; Lizzit, S. Growth of Dome-Shaped Carbon Nanoislands on Ir(111): The Intermediate Between Carbidic Clusters and Quasi-Free-Standing Graphene. *Phys. Rev. Lett.* **2009**, *103*, 166101.

(38) Preobrajenski, A. B.; Ng, M. L.; Vinogradov, A. S.; Mårtensson, N. Controlling Graphene Corrugation on Lattice-Mismatched Substrates. *Phys. Rev. B* **2008**, *78*, 073401.

(39) Presel, F.; Jabeen, N.; Pozzo, M.; Curcio, D.; Omiciuolo, L.; Lacovig, P.; Lizzit, S.; Alfè, D.; Baraldi, A. Unravelling the Roles of Surface Chemical Composition and Geometry for the Graphene–Metal Interaction through C1s Core-Level Spectroscopy. *Carbon* **2015**, *93*, 187-198.

(40) Susi, T.; Kaukonen, M.; Havu, P.; Ljungberg, M. P.; Ayala, P.; Kauppinen, E. I. Core Level Binding Energies of Functionalized and Defective Graphene. *Beilstein J. Nanotechnol.* **2014**, *5*, 121–132.

(41) Baraldi, A. Structure and Chemical Reactivity of Transition Metal Surfaces as Probed by Synchrotron Radiation Core Level Photoelectron Spectroscopy. *J. Phys.: Condens. Matter* **2008**, *20*, 093001.

(42) Baraldi, A.; Cerdá, J.; Martin-Gago, J. A.; Comelli, G.; Lizzit, S.; Paolucci, G.; Rosei, R. Oxygen Induced Reconstruction of the Rh(100) Surface: General Tendency towards Threefold Oxygen Adsorption Site on Rh Surfaces. *Phys. Rev. Lett.* **1999**, *82*, 4874-4877.

(43) Ganduglia-Pirovano, M. V.; Scheffler, M.; Baraldi, A.; Lizzit, S.; Comelli, G.; Paolucci, G.; Rosei, R. Oxygen-Induced Rh $3d_{5/2}$ Surface Core-Level Shifts on Rh(111). *Phys. Rev. B* **2001**, *63*, 205415.

(44) Lizzit, S.; Baraldi, A.; Groso, A.; Reuter, K.; Ganduglia-Pirovano, M. V.; Stampfl, C.; Scheffler, M.; Stichler, M.; Keller, C.; Wurth, W.; *et al.* Surface Core-Level Shifts of Clean and Oxygen-Covered Ru (0001). *Phys. Rev. B* **2001**, *63*, 205419.

(45) Baraldi, A.; Lizzit, S.; Comelli, G.; Paolucci, G. Oxygen Adsorption and Ordering on Ru(1010). *Phys. Rev. B* **2001**, *63*, 115410.

(46) Bianchettin, L.; Baraldi, A.; de Gironcoli, S.; Lizzit, S.; Petaccia, L.; Vesselli, E.; Comelli, G.; Rosei, R. Geometric and Electronic Structure of the N-Rh (100) System by Core-Level Photoelectron Spectroscopy: Experiment and Theory. *Phys. Rev. B* **2006**, *74*, 045430.

(47) Bianchettin, L.; Baraldi, A.; Vesselli, E.; de Gironcoli, S.; Lizzit, S.; Petaccia, L.; Comelli, G.; Rosei, R. Experimental and Theoretical Surface Core Level Shift Study of the S-Rh(100) Local Environment. *J. Phys. Chem. C* **2007**, *111*, 4003-4013.

(48) Weststrate, C. J.; Baraldi, A.; Rumiz, L.; Lizzit, S.; Comelli, G.; Rosei, R. A Surface Core Level Shift Study of Hydrogen Interaction with Rh(111). *Surf. Sci.* **2004**, *566–568*, 486-491.

(49) Tetlow, H.; Posthuma de Boer, J.; Ford, I. J.; Vvedensky, D. D.; Curcio, D.; Omiciuolo, L.; Lizzit, S.; Baraldi, A.; Kantorovitch, L. Ethylene Decomposition on Ir(111): Initial Path to Graphene Formation. *Phys. Chem. Chem. Phys.* **2016**, *18*, 27897-27909.

(50) Tetlow, H.; Ford, I. J.; Kantorovich, L. A Free Energy Study of Carbon Clusters on Ir(111): Precursors to Graphene Growth. *J. Chem. Phys.* **2017**, *146*, 044702.

(51) Ferrari, E.; Galli, L.; Miniussi, E.; Morri, M.; Panighel, M.; Ricci, M.; Lacovig, P.; Lizzit, S.; Baraldi, A. Layer-Dependent Debye Temperature and Thermal Expansion of Ru(0001) by Means of High-Energy Resolution Core Level Photoelectron Spectroscopy. *Phys. Rev. B* **2010**, *82*, 195420.

(52) Föhlisch, A.; Wassdahl, N.; Hasselström, J.; Karis, O.; Menzel, D.; Mårtensson, N.; Nilsson, A. Beyond the Chemical Shift: Vibrationally Resolved Core-Level Photoelectron Spectra of Adsorbed CO. *Phys. Rev. Lett.* **1998**, *81*, 1730-1733.

(53) Niimi, Y.; Matsui, T.; Kambara, H.; Tagami, K.; Tsukada, M.; Fukuyama, H. Scanning Tunneling Microscopy and Spectroscopy of the Electronic Local Density of States of Graphite Surfaces Near Monoatomic Step Edges. *Phys. Rev. B* **2006**, *73*, 085421.

(54) Huang, J. Y.; Ding, F.; Yakobson, B. I.; Lu, P.; Qi, L.; Li, J. In Situ Observation of Graphene Sublimation and Multi-Layer Edge Reconstructions. *Proc. Natl. Acad. Sci. U. S. A.* **2009**, *106*, 10103–10108.

(55) McCarty, K. F.; Feibelman, P. J.; Loginova, E.; Bartelt, N. C. Kinetics and Thermodynamics of Carbon Segregation and Graphene Growth on Ru(0 0 0 1). *Carbon* **2009**, *47*, 1806-1813.

(56) Batzill, M. The Surface Science of Graphene: Metal Interfaces, CVD Synthesis, Nanoribbons, Chemical Modifications, and Defects. *Surf. Sci. Rep.* **2012**, *67*, 83-115.

(57) Miniussi, E.; Pozzo, M.; Baraldi, A.; Vesselli, E.; Zhan, R. R.; Comelli, G.; Menteş, T. O.; Niño, M. A.; Locatelli, A.; Lizzit, S.; *et al*. Thermal Stability of Corrugated Epitaxial Graphene Grown on Re(0001). *Phys. Rev. Lett.* **2011**, *106*, 216101.

(58) Miniussi, E.; Pozzo, M.; Mentes, T. O.; Niño, M. A.; Locatelli, A.; Vesselli, E.; Comelli, G.; Lizzit, S.; Alfè, D.; Baraldi, A. The Competition for Graphene Formation on

Re(0001): A Complex Interplay between Carbon Segregation, Dissolution and Carburisation. *Carbon* **2014**, *73*, 389-402.

(59) Gao, J.-H.; Ishida, N.; Scott, I.; Fujita, D. Controllable Growth of Single-Layer Graphene on a Pd(1 1 1) Substrate. *Carbon* **2012**, *50*, 1674-1680.

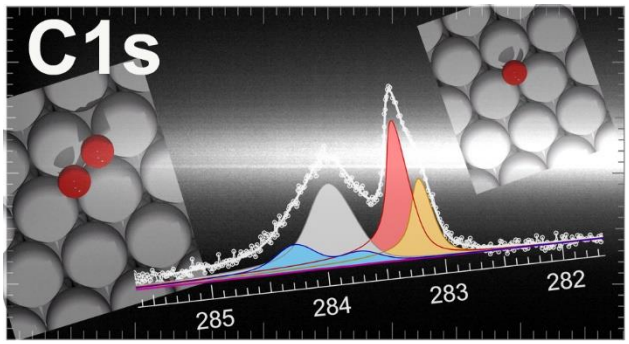

TOC Graphic